JOURNAL OF APPLIED ELECTROCHEMISTRY 24 (1994) 1133–1138

Photoelectrochemical properties of bismuth-doped titanium oxide electrodes

S.-Y. PARK, B.-W. CHO, K.-S. YUN

Electrochemistry Laboratory, KIST, PO Box 131, Cheongryang, Seoul, Korea

E.-C. LEE

Department of Metallurgical Engineering, Korea University, 1 Anam Dong, Seoul, Korea

Received 23 November 1993; revised 15 April 1994

With the aim of obtaining TiO_2 films with increased photoresponse titanium metal was alloyed with bismuth and then directly oxidized. The free energy efficiencies of the Ti–Bi oxide increased four times by increasing the bismuth content up to 10 wt %. The spectral response of the Ti–Bi oxides was slightly shifted toward the visible region with respect to the response of TiO_2, and their E_g were observed to be in the range 2.87–3.0 eV.

1. Introduction

To obtain photoelectrodes of practical interest, the bandgap must be minimized and, at the same time, the flatband potential must be optimized [1]. This is particularly true in the case of semiconductors for water photoelectrolysis, whose forbidden band has to match the solar spectrum, as well as the H^+/H_2 and O_2/H_2O redox levels.

A great deal of attention has recently been paid to the photoelectrochemical (PEC) conversion of solar energy to electrical power or a storable energy form, for example, hydrogen. The photoelectrolysis of water using semiconductor electrodes has received significant attention in the past decade. In initial and subsequent studies, n-TiO_2 has been shown to be exceptionally stable with high quantum efficiency ($\sim 100\%$). However, its optical band gap ($E_g \sim 3$ eV) is a disadvantage with regard to its application as a photoelectrode in solar powered photoelectrolysis systems. Most of the small bandgap oxide and nonoxide semiconductors investigated were found to exhibit either photocorrosion or unsuitable flatband potential. After an extensive search for suitable semiconductors over the period from 1972 to 1985; an interest in TiO_2 has developed [2]. Several different approaches are being pursued to circumvent the poor solar spectral response of TiO_2 caused by its large bandgap. The bandgap can be reduced by alloying with VO_2 [3]. Similarly, to improve its limited solar response TiO_2 mixed oxide alloys such as TiO_2–SiO_2 [4], TiO_2–NbO_2 [5] and TiO_2–Co_3O_4 [6] have been studied knowing that the binary oxide catalysts show higher activity than their components. As the doping level depends on the dopant oxide solubility in TiO_2, a solubility greater than 0.01% has been recommended for effective doping [7]. Recently, a new procedure has been followed, namely, the direct oxidation of titanium alloys.

With the aim of obtaining films with increased photoresponse, we have attempted the direct oxidation of titanium alloys. In this paper the influence of the alloying element bismuth on the oxide film photoresponse and its optical band gap, E_g, is considered. The cause for the increase in photocurrent with the increase in donor density is also discussed on the basis of depletion-layer photoeffects.

2. Experimental details

2.1. *Synthesis*

Titanium–bismuth alloys of five different compositions (1, 5, 10, 15, 20 wt % Bi) were prepared by mixing the appropriate amounts of titanium (Aldrich, 99.9%) and bismuth (Aldrich, 99.99%) powders. The mixture was pressed at 3200 psi to form a cylindrical pellet. The pellet was melted, to give a homogeneous alloy, in an argon arc furnace under reduced pressure. The ingots were annealed at 900° C under reduced pressure (10^{-4} torr) to ensure homogeneity of the samples. The ingots were cut into discs (10 mm diam. × 2 mm thickness), with a diamond wheel saw (South Bay Technology M650). The samples were mechanically polished to a mirror finish with SiC paper (400 to 1200) and 0.05 μm alumina successively. The polished samples were oxidized by exposing to air in an electric furnace at 800° C for 10 min.

2.2. *Characterization*

Structural characterization of the oxidized films was performed with an X-ray diffractometer operated at 30 kV, 15 mA using CuK_α radiation.

The electrodes were connected to enamel coated pure copper wire with silver epoxy and sealed with silicone rubber leaving an exposed area of 1 cm^2. The

Table 1. d-spacing (nm) and peak intensity in X-ray diffraction analysis of Ti–Bi oxide electrodes

Bi1%	*Bi5%*	*Bi10%*	*Bi15%*	*Bi20%*	*Ti*	*Ti_2O*	*TiO*	*TiO_2*	*$Bi_2Ti_4O_{11}$*	*$Bi_4(TiO_4)_3$*
0.3256 (24)	0.3251 (100)	0.3256 (31)	0.3246 (26)	0.3250 (20)	–	–	–	0.325 (100)	–	–
0.2565 (20)	0.2568 (18)	0.2567 (50)	0.2567 (87)	0.2563 (100)	–	–	0.256 (100)	–	–	–
0.2499 (9)	0.2492 (37)	0.2490 (9)	0.2487 (18)	0.2489 (10)	–	–	–	0.2487 (50)		–
–	–	0.2447 (7)	0.2443 (6)	0.2449 (3)	–	–	–	–	0.2429 (25)	–
0.2378 (13)	0.2365 (14)	0.2377 (23)	0.2375 (12)	0.2372 (5)	0.2342 (20)	–	–	–	–	–
–	–	0.2304 (9)	0.2301 (10)	0.2296 (7)	–	–	–	0.2297 (8)	–	–
0.2259 (100)	0.2253 (98)	0.2260 (100)	0.2257 (95)	0.2252 (82)	0.2244 (100)	–	–	–	–	–
0.2195 (6)	0.2188 (14)	0.2188 (5)	0.2187 (7)	0.2186 (5)	–	–	–	0.2188 (25)	–	–
–	–	–	0.2053 (2)	0.2051 (3)	–	–	–	–	–	0.205 (1)
0.1739 (33)	0.1735 (21)	0.1739 (29)	0.1738 (12)	0.1739 (7)	0.1726 (19)	–	–	–	–	–
–	0.1687 (25)	0.1688 (7)	0.1688 (13)	0.1687 (10)	–	–	–	0.16874 (60)	–	–
–	0.1624 (10)	0.1624 (4)	0.1625 (5)	0.1622 (2)	–	–	–	0.16237 (20)	–	–
0.1478 (31)	0.1478 (13)	0.1481 (8)	0.1479 (60)	0.1478 (57)	–	–	0.1474 (80)	–	–	–
0.1345 (17)	0.1359 (12)	0.135 (4)	0.1358 (10)	0.1359 (7)	–	–	–	0.13598 (20)	–	–
–	–	–	0.1282 (17)	0.1280 (15)	–	0.1281 (20)	–	–	–	–
0.1254 (5)	–	0.1252 (23)	–	–	–	0.1239 (60)	–	–	–	–

sealant has been observed to be stable in 1 M NaOH. Photoelectrochemical characterization of the electrodes was performed by measuring the current–potential characteristics. The PEC measurements were carried out in a conventional three-electrode glass cell with a quartz window. A platinum wire was used as counter electrode and a saturated calomel electrode as reference electrode. All PEC experiments were done in nitrogen-purged 1M NaOH at room temperature. All the reagents were analytical grade and prepared with ultra pure water (18 MΩ cm).

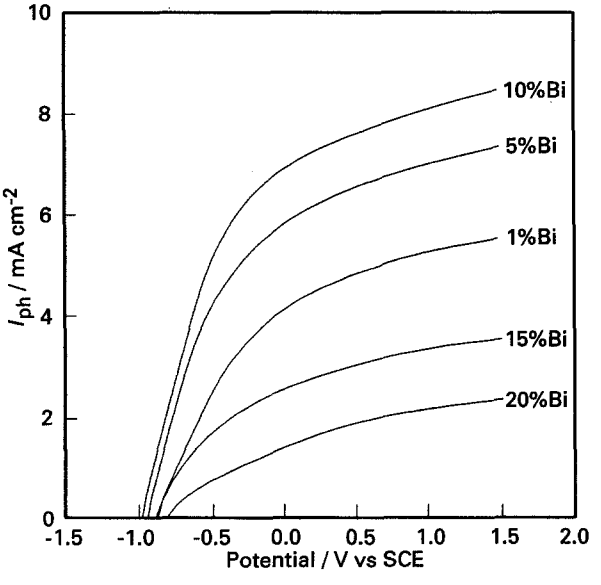

Fig. 1. I_{ph}/V curves of Ti–Bi oxide electrodes under illumination by white light. ($W_a = 0.2\,W\,cm^{-2}$)

The current–potential curves were obtained with a potentiostat (Princeton Applied Research, model 273) using the potentiodynamic mode. The impedance measurements were taken under potentiostatic control by superimposing an a.c. voltage of 5 mV amplitude on a d.c. potential ranged between −1.0 and 1.5 V vs SCE using a Solartron 1255 frequency response analyser.

The light source was a 150 W xenon arc lamp (Oriel Co. 6254) in a lamp housing (Oriel Co. 66057) with a water filter to remove heating effects. The light intensity was measured to be $0.2\,W\,cm^{-2}$ with a photodetector (Spectra Physics 405). A set of neutral density filters was employed for changing the light intensity. Measurements with monochromatic light were made using a grating monochromator placed between the light source and the cell.

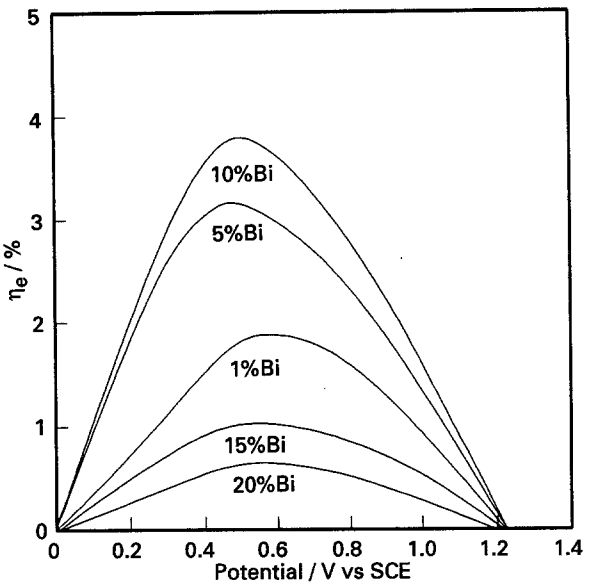

Fig. 2. Effect of applied bias voltage on the sunlight conversion energy efficiency of Ti–Bi oxide electrodes under illumination by white light. ($W_a = 0.2\,W\,cm^{-2}$).

3. Results and discussion

3.1. *Structural characteristics*

Structural characterization of oxidized Ti–Bi films was performed. The values for peak positions and their relative intensities are given in Table 1. Also listed therein are the standard 'd' values for TiO_2, Ti, Ti_2O, TiO, $Bi_2Ti_4O_{11}$ and $Bi_4(TiO_4)_3$ for comparison with the observed intensities. Comparing the 'd' value for the observed equiatomic composition with the standard values for lattice spacing (above) it may be concluded that the oxide layers for all the specimens contain a mixture of TiO_2, Ti, Ti_2O, TiO, $Bi_2Ti_4O_{11}$ and $Bi_4(TiO_4)_3$. According to a model suggested by Paleolag *et al.* [8] the oxide layer is composed mainly of TiO_2 (rutile) on the outer side. The presence of TiO_2 on the outermost layer of the electrode has been confirmed by the spectral response measurements of the PEC cells formed with the Ti–Bi oxide electrode. The E_g values calculated from these results are similar to that of TiO_2.

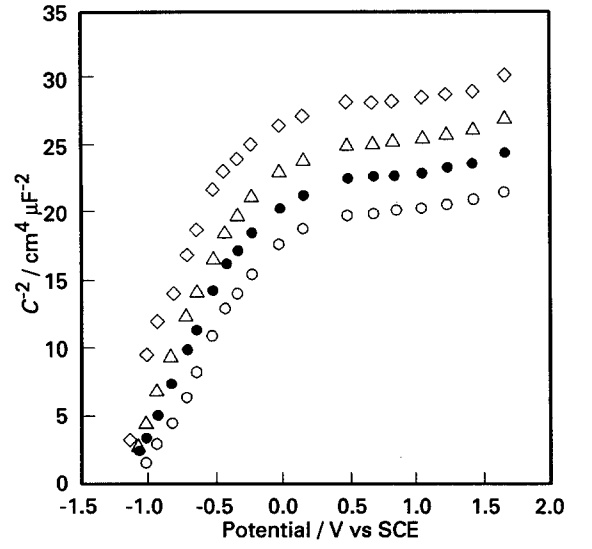

Fig. 3. Mott–Schottky plots for the 15Bi electrode. Frequency/kHz: (○) 0.25, (●) 0.63, (△) 1.6 and (◇) 4.0.

3.2. *Photocurrent–potential characteristics*

Figures 1 and 2 show the photocurrent density–potential curve and the free energy efficiency (η_e) under illumination with 150 W xenon lamp for the oxidized Ti–Bi electrodes. The η_e values for the photoanode were calculated using the equation [9]:

$$\eta_e = \frac{I_{ph}(1.23 - V_a)}{W_a} \times 100\% \qquad (1)$$

where V_a is the applied potential (V) and W_a is the incident light intensity ($W\,cm^{-2}$). η_e is strongly dependent on the magnitude of the bias voltage. Electrode 10Bi (oxidized Ti–Bi alloy with 10 wt % Bi) was shown to have a maximum η_e value of 3.9%, with a bias of 0.5 V. The potential at which the onset of photocurrent takes place (V_{on}) is particularly important since it enables us to position the conduction band edge (E_c) of the semiconductors on the energy scale of the reference. This is particularly important in cases where the linearity of the Mott–Schottky plot is limited to a narrow range, thus making the determination of the flatband potential inaccurate.

3.3. *Impedance analysis*

Mott–Schottky plots of the Ti–Bi oxide with 15% weight content of bismuth are shown in Fig. 3, at different increasing frequencies. This behaviour is based on the following mathematical relationship [10]:

$$\frac{1}{C_{sc}^2} = \frac{2}{q\epsilon\epsilon_0 N_d A^2}\left(V - V_{fb} - \frac{kT}{q}\right) \qquad (2)$$

where C_{sc} is the space charge layer capacitance per unit area, A is the actual electrode area, q is the electronic charge, ϵ and ϵ_0 are the dielectric constants of the semiconductor and of the vacuum, respectively, N_d is the donor density, V is the electrode potential, and V_{fb} is the flatband potential. A linear relationship between inverse squared space charge capacitance, $1/C_{sc}^2$, and applied potential, V, is found to hold only in the applied potential range from $1/C_{sc}^2 = 0$ to the inflection point, and the slopes of the $1/C_{sc}^2$ against V plot decrease gradually with increasing applied potential in the range of applied potential more positive than at the inflection point, irrespective of the measuring frequency and bismuth content. In the applied potential range from $1/C_{sc}^2 = 0$ to the inflection point, N_d is calculated from the slope of $1/C_{sc}^2$ against V, while V_{fb} is obtained by extrapolation of the linear part. In the case of bulk semiconducting crystals, a linear Mott–Schottky plot was generally obtained [11], but in thin film semiconductors, a nonlinear Mott–Schottky plot is obtained [12].

Table 2 shows N_d and V_{fb} obtained from the Mott–Schottky plots and V_{on} obtained from the I_{ph}/V plot with different contents of bismuth. V_{fb} shifted slightly

Table 2. Onset potential, flatband potential and donor density of oxidized Ti–Bi electrodes

Electrode	V_{on}/V	V_{fb}/V	$10^{20}N_d$/cm^3
1Bi	−0.85	−1.04	26.1
5Bi	−0.92	−1.17	94.7
10Bi	−0.95	−1.22	115.1
15Bi	−0.87	−1.13	6.4
20Bi	−0.80	−0.98	3.6

toward negative values and N_d increased with increasing bismuth concentration to 10 wt %. The onset potential, V_{on}, is always more anodic than the flatband potential determined from Mott–Schottky plots, the difference depending on the recombination efficiency of the photogenerated carriers in the near flatband condition [13]. N_d was increased by increasing the bismuth concentration but decreased above 10 wt % bismuth.

From impedance measurement, the electrical resistance (R) of Ti–Bi oxide with varying bismuth content was determined from Nyquist and Bode (impedance against frequency) plots. Figure 4 shows R against percentage Bi obtained from the Bode and Nyquist plots. The electrical resistance showed a tendency to decrease slightly with increase of bismuth to 10 wt % but to increase drastically above 10 wt %. Increasing the content of bismuth results in an increase of N_d. R plays an important role in the ohmic drop in the semiconductor, eventually limiting the overall photocurrent of the cell. Above 10 wt % Bi, R became much higher than that below 10 wt % Bi. For this reason, when the impedance experiment was performed, compared to small R, the measured current was changed at a given d.c. potential. Therefore, the capacitance value was not calculated under the same conditions as that at below 10 wt % Bi. That is, the slope of the Mott–Schottky plot is not accurate in the case of high R. The calculated N_d will be smaller than the real N_d.

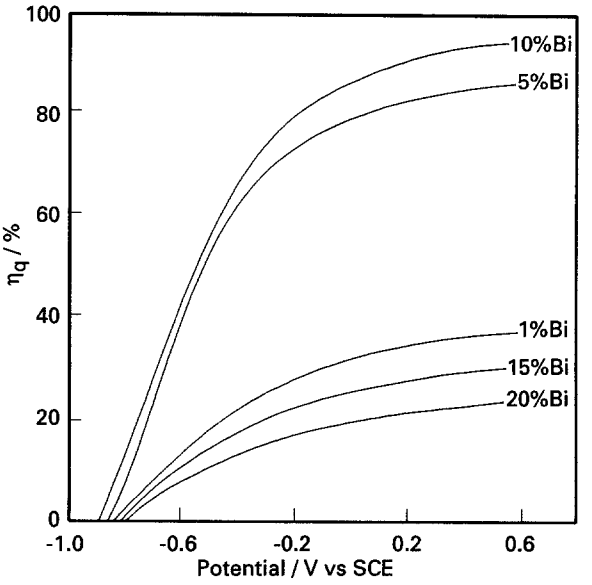

Fig. 5. η_q/V curves of Ti–Bi oxide electrodes under illumination by monochromatic light ($\lambda = 310$ nm).

3.4. *Spectral response*

Quantum efficiencies (η_q) of the photoanode were calculated using the equation [14]:

$$\eta_q = \frac{\text{No. of electrons}}{\text{No. of photons}} \times 100\% \qquad (3)$$

Figure 5 shows typical photocurrent density against quantum efficiency curves at 310 nm. Depending on the increase of potential, the curve shows an increase in the quantum efficiency at first, then a gradual saturation. Furthermore, η_q increased with increasing bismuch content to 10 wt % Bi. If the bismuth content was increased any further, the curve showed a decreasing trend. The bandgap of Ti–Bi oxide electrodes was determined from an I_{ph} against wavelength plot. Figure 6 clearly indicates no significant shift in bandgap of Ti–Bi oxides regardless of the bismuth content. On increasing the energy of the incident

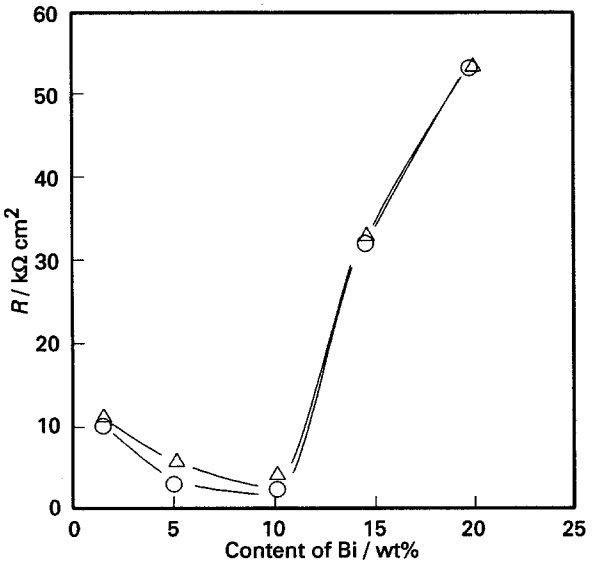

Fig. 4. R against content of bismuth obtained from Bode (○) and Nyquist (△) plots.

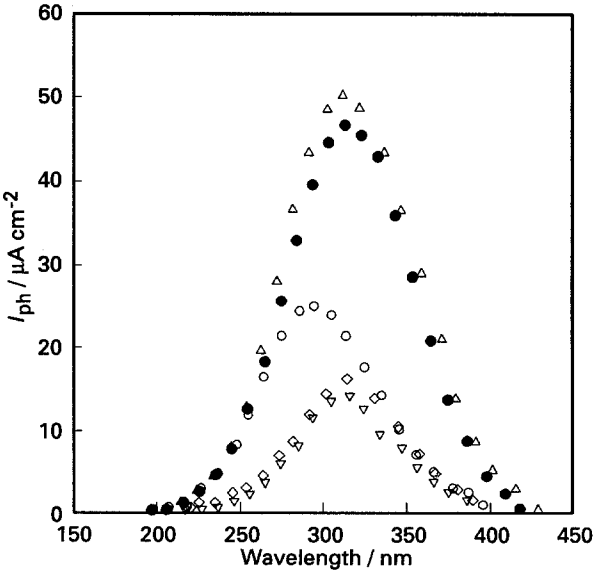

Fig. 6. I_{ph}/λ plot for Ti–Bi oxide electrodes. Wt % Bi: (○) 1%, (●) 5%, (△) 10%, (◇) 15% and (▽) 20%.

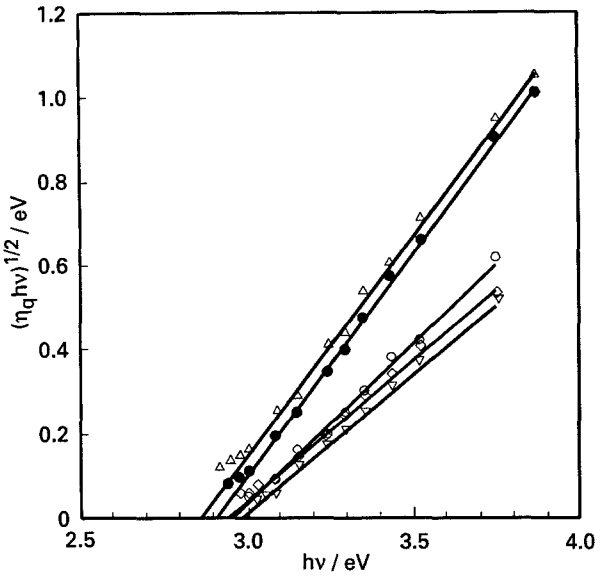

Fig. 7. Determination of V_{fb} from the variation of I_{ph}^2 with applied potential for Ti–Bi oxide electrodes. Wt % Bi: (○) 1%, (●) 5%, (△) 10%, (◇) 15% and (▽) 20%.

light, the photoresponse increased to 3.9 eV, then decreased above 3.9 eV. In this study, the Ti–Bi oxide electrode was illuminated by a 150 W xenon lamp and the spectral irradiance of this lamp was decreased drastically below 310 nm (4.0 eV). Agustynski *et al.* [15] have attributed the improved I/V characteristics and the increased anode stability of their TiO_2–Al_2O_3 electrodes over TiO_2 to the lower electrical resistivity of mixed oxide coatings. With the aim of exactly evaluating the bandgap energy of the Ti–Bi oxide alloy, $(\eta_q h\nu)^{1/2}$ was plotted as a function of the photon energy. The lines of Fig. 7 show a linear least-squares fit to the data points, yielding a bandgap in the 2.85–3.02 eV range.

Figure 8 shows the dependence of photocurrent density on the time of continuous illumination. Except for a small decay in the first few hours of illumination, the Ti–Bi oxide showed no decay in

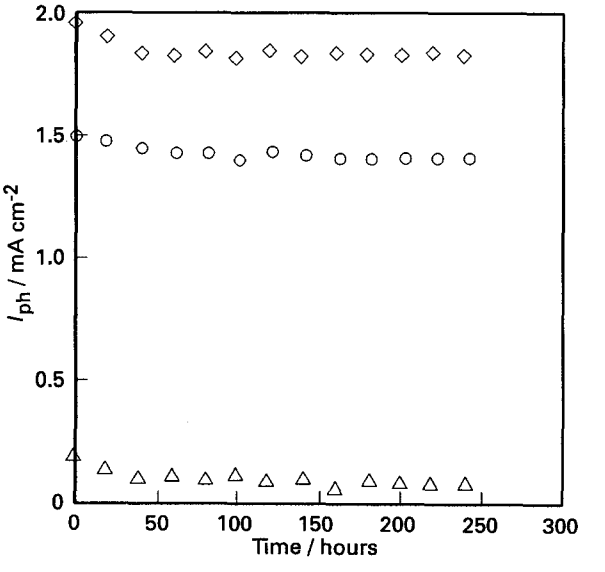

Fig. 8. I_{ph} for Ti–Bi oxide electrodes as a function of time during continuous white light illumination (150 W xenon lamp) at −0.87 V vs SCE. Wt % Bi: (△) 1%, (○) 5% and (◇) 10%.

Table 3. Various parameters of oxidized Ti–Bi electrodes

Electrode	$10^8\alpha^{-1}$/cm	$10^8 W_0$/cm	ϵ	αW_0	αL_p
1Bi	46.9	20.6	100	0.52	0.22
5Bi	7.5	15.8	190	2.16	1.01
10Bi	4.1	12.1	153	3.08	1.85
15Bi	149.2	47.7	132	0.41	0.04
20Bi	185.2	72.9	173	0.40	0.03

photocurrent for 240 h of continuous operation. Scanning Auger electron microscope (SAM) analysis of the electrode surface before and after 240 h of illumination showed no flaking off or other physical damage to the film.

3.5. *Theoretical analysis of photocurrent change*

The Gartner theory of depletion-layer photoeffects describes photocurrents in photoelectrochemical cells using large bandgap semiconductors. According to this theory, the semiconductor–electrolyte interface is treated as a simple Schottky barrier. Using this model, Kennedy and Frese [16] found the following relationship between photocurrent efficiencies and semiconductor solid–state parameters:

$$\ln(1-\eta_q) = -\alpha\left(\frac{2\epsilon\epsilon_0}{qN_d}\right)^{1/2}(V-V_{fb})^{1/2} - \ln(1+\alpha L_p) \quad (4)$$

where α is the optical absorption coefficient, L_p is the hole diffusion length. Equations 2 and 4 show that the values α, ϵ, W and L_p cannot be obtained independently. Thus, the ϵ value of TiO_2(= 170) [17] was substituted into Equation 2, so that N_d for the oxidized Ti–Bi can be calculated from Equation 4; α, L_p and W_0 can thus be obtained. After calculating the TiO_2 parameter values, the intermediate values, L_p of the bismuth-doped TiO_2, were not significantly different from the value of undoped titanium oxide (7.6×10^{-8} cm). Therefore, from Equations 2 and 4, ϵ, α, N_d and W_0 can be obtained: their values are listed in Table 3. From Gartner's photocurrent density equation [18], the doped TiO_2 electrode photocurrent increase is due to increase in the donor density, followed by the hole generations in the depletion layer (J_{dep}) and in the diffusion layer (J_{diff}). It can be noticed that the percentage increase in photocurrent in the depletion layer is greater than that in the diffusion layer.

4. Conclusion

Ti–Bi alloys of five different compositions (1, 5, 10, 15, 20 wt % Bi) were prepared in an arc furnace and were oxidized in an electric furnace at 800° C for 10 min. The X-ray diffraction technique showed that the oxide layers for all the specimens contained a mixture of TiO_2, Ti_2O, TiO, $BiTiO_3$ and Bi_2Ti_4O. The oxide layer was composed mainly of TiO_2 on the outer side. The free energy efficiency of Ti–10Bi

oxide was 3.9%, which was four times higher than that of TiO_2. the spectral response of Ti–Bi oxide was similar to the response of the TiO_2 and its E_g was observed to be 3.0–2.87 eV. The quantum efficiencies (η_q) of Ti–Bi oxide films increased with the applied bias voltage and were observed to be in the range 25 ~ 95% at 0.5 V vs SCE.

The cause of the increase in photocurrent with increase in donor density can be due to carriers generated within the depletion layer and those carriers generated in the bulk that diffuse into the depletion layer. With increase in donor density, the percentage increase of J_{dep} is much larger than that of J_{diff}.

References

[1] A. J. Nozik, *Faraday Discuss. Chem. Soc.* **70** (1981) 7.
[2] K. J. Hartig and N. Getoff, 'Hydrogen Energy Progress VI', Pergamon Press, New York (1986) p. 546.
[3] T. C. Philips, K. Moorjani, J. C. Murphy and T. O. Poehler, *J. Electrochem. Soc.* **129** (1982) 1210.
[4] Masakazu, Anpo, N. Hiroki, K. Sukeya, K. Yutaka, Kuzunaridomen and T. Haruonishi, *J. Phys. Chem.* **90** (1980) 1633.
[5] J. Gautron, P. Lamasson, B. Poumellec and J. F. Marucco, *Sol. Energy Mater.* **9** (1983) 101.
[6] S. Zielinski, A. Sobczynski, *Acta Chim. Hung.* **120** (1985) 229.
[7] V. Guruswamy and J. O'M. Bockris, *ibid.* **1** (1979) 411.
[8] E. Paleolag, A. Fedotova, O. Derjagina and N. Tomashov, *J. Electrochem. Soc.* **125** (1978) 1410.
[9] A. K. Ghosh and H. P. Maruska, *ibid.* **124** (1977) 1516.
[10] H. Gerischer, *Adv. Electrochem. Electrochem. Eng.* **1** (1961) 139.
[11] J. F. Dewald, *Bell Syst. Tech. J.* **39** (1960) 615.
[12] J. F. McAleer and L. M. Peter, *J. Electrochem. Soc.* **129** (1982) 1252.
[13] M. A. Butler, *Mater. Sci.* **15** (1980) 1.
[14] K. V. C. Rao, M. R. Rao, M. P. Nair, V. G. Kumar and C. G. R. Nair, *Int. J. Hydrogen Energy* **14**(5) (1989) 295.
[15] J. Augustynski, J. Hinden and C. Stalder, *J. Electrochem. Soc.* **124** (1977) 1063.
[16] J. H. Kennedy and K. W. Frese, *ibid.* **123** (1976) 1683.
[17] F. A. Grant, *Ref. Modern Phys.* **31** (1959) 646.
[18] W. W. Gartner, *Phys. Rev.* **116** (1959) 84.